# Electromagnetic backscattering from one-dimensional drifting fractal sea surface I: Wave–current coupled model*

Tao Xie(谢涛)[1,2,†], Shang-Zhuo Zhao(赵尚卓)[1,2], William Perrie[3], He Fang(方贺)[1,2], Wen-Jin Yu(于文金)[1,2], and Yi-Jun He(何宜军)[1,2]

[1] School of Marine Sciences, Nanjing University of Information Science and Technology, Nanjing 210044, China
[2] Jiangsu Engineering Technology Research Center of Marine Environment Detection, Nanjing 210044, China
[3] Fishreis & Oceans Canada, Bedford Institute of Oceanography, Dartmouth, Nova Scotia, B2Y 4A2 Canada

(Received 20 October 2015; revised manuscript received 12 January 2016; published online 20 April 2016)

To study the electromagnetic backscattering from a one-dimensional drifting fractal sea surface, a fractal sea surface wave–current model is derived, based on the mechanism of wave–current interactions. The numerical results show the effect of the ocean current on the wave. Wave amplitude decreases, wavelength and kurtosis of wave height increase, spectrum intensity decreases and shifts towards lower frequencies when the current occurs parallel to the direction of the ocean wave. By comparison, wave amplitude increases, wavelength and kurtosis of wave height decrease, spectrum intensity increases and shifts towards higher frequencies if the current is in the opposite direction to the direction of ocean wave. The wave–current interaction effect of the ocean current is much stronger than that of the nonlinear wave–wave interaction. The kurtosis of the nonlinear fractal ocean surface is larger than that of linear fractal ocean surface. The effect of the current on skewness of the probability distribution function is negligible. Therefore, the ocean wave spectrum is notably changed by the surface current and the change should be detectable in the electromagnetic backscattering signal.

**Keywords:** fractal, ocean surface current, ocean wave, NRCS

**PACS:** 41.20.Jb, 84.40.Xb, 91.50.Iv, 92.10.Hm **DOI:** 10.1088/1674-1056/25/6/064101

## 1. Introduction

There are many types of ocean currents with different spatial and temporal scales on the ocean surface. They are essential components of the ocean circulation system and the relevant ecosystem. Ocean currents play important roles in the transportation of heat, mass, momentum, nutrients and energy.[1]

Remote sensing by satellite is the ideal technology for studying hydrodynamic dynamics of the ocean surface. It can obtain daily and weekly global coverage data with high revisit frequency and high spatial resolution by synthetic aperture radar (SAR). Chapron *et al.*,[2] and Johannessen *et al.*[3] derived an indirect retrieval algorithm for ocean surface current from the SAR Doppler frequency shift, as observed in the imagery. This method can only retrieve ocean current velocity in the range direction and the current direction is only derived with the aid of ancillary information. Marghany[4] improved the retrieval method for ocean current for RADARSAT-1 measurements by SAR imagery through using a method based on wavelength discrepancy and multiple looks at different frequencies. Some relevant studies and publications have reported ocean current retrieval results in different geographical areas by using TerraSAR-X, and Envisat ASAR.[5,6] Unfortunately, there is no method to directly measure ocean currents by sensors on satellites presently.

For ocean surface current, it is necessary to study the remote sensing mechanism, where the effect of the ocean current on electromagnetic (EM) backscattering of the sea surface is a key step to solve the problem. The surface current can modulate the EM backscattering signal because the current can change the wave parameters such as wave spectrum, wave height, wave period and other relevant variables. As a case study, the shoaling wave experiment (SHOWEX) shows that there is a drift of the wind wave spectrum with the mean wind direction because of horizontal current shear at the edge of the current front.[7] Therefore, there is an obvious correction of the amplitude dispersion relation, which is needed in the shallow water area.[8] Numerical results for the time evolution of the shallow water wave show that offshore currents can occur when a wave propagates and breaks in topographically changing shallow water, whereas the intensity and scale of the offshore current can be weakened by negative feedback because of the wave–current interaction.[9]

A fundamental objective of our study is to establish a high accuracy sea surface model. The fractal geometry method has characteristics of both periodicity and stochasticity. It can

*Project supported by the National Natural Science Foundation of China (Grant No. 41276187), the Global Change Research Program of China (Grant No. 2015CB953901), the Priority Academic Development Program of Jiangsu Higher Education Institutions (PAPD), Program for the Innovation Research and Entrepreneurship Team in Jiangsu Province, China, the Canadian Program on Energy Research and Development, and the Canadian World Class Tanker Safety Service.

†Corresponding author. E-mail: xietao@nuist.edu.cn

© 2016 Chinese Physical Society and IOP Publishing Ltd 

therefore be easily used to simulate the sea surface. Many recent studies focused on the fractal sea surface model and have used this approach to study EM scattering at the sea surface.[10–17] In this paper, the one-dimensional linear and nonlinear fractal sea surface models are used to derive wave–current coupled models, based on the wave–current interaction mechanism.

Nonlinear wave–current coupled models are derived in Section 2. An error analysis of our models is given in Section 3. Numerical simulation of the effect of the ocean current on the waves is given in Section 4. Conclusions are shown in Section 5.

## 2. One-dimensional wave–current coupled models

Starting with linear and nonlinear fractal sea surface models, linear and nonlinear wave–current models are derived in this section.

### 2.1. Linear fractal sea surface

For a one-dimensional linear irrotational flow system, the velocity potential function is

$$\Phi(x,t) = \varphi(x)\,\mathrm{e}^{\mathrm{i}\omega t}, \tag{1}$$

where $\omega$ is the radian frequency of the ocean wave. The linear wave derived from Eq. (1) is given by

$$f_{\text{linear}}(x,t) = \sum_{n=1}^{N} a_n \sin\Psi_n, \tag{2}$$

where $N$ is the number of wave components, $\Psi_n = k_n x - \omega_n t + \varphi_n$, $a_n$, $k_n$, $\omega_n$, and $\varphi_n$ are the amplitude, wave number, radian frequency, and phase of the $n$-th wave components, respectively. A given wave propagates in the $x$ direction. Time is represented by $t$ in units of seconds. Wave numbers are given by

$$k_n = 2\pi/\lambda_n, \tag{3}$$

where $\lambda_n$ is wavelength of the $n$-th wave component. The dispersion relationship in deep water is

$$\omega_n = \sqrt{gk_n}, \tag{4}$$

where $g = 9.8\ \mathrm{m\cdot s^{-1}}$ is the acceleration due to gravity. According to the literature,[10] the one-dimensional linear fractal sea surface height is given by

$$f_{\text{linear}}(x,t) = \sigma C \sum_{n=0}^{N-1} b^{(s-2)n} \sin(k_0 b^n x - \omega_n t + \varphi_n), \tag{5}$$

where $k_0 = 2\pi/\lambda_0$ is the dominant wave number; $\lambda_0$ is the dominant wavelength (the maximum wavelength in Eq. (2)); $b(b>1)$ is a scale factor for amplitude and frequency; $f(x,t)$ is a periodic function when $b$ is a rational number, and $f(x,t)$ is a non-periodic function if $b$ is an irrational number; $\sigma$ is the standard deviation of $f(x,t)$, which is related to significant wave height $h_{\mathrm{s}}$ by the relation, $\sigma = h_{\mathrm{s}}/4$; $C = \sqrt{2[1-b^{2(s-2)}]/1-b^{2N_f(s-2)}}$; $s$ $(1<s<2)$ is the roughness coefficient of the fractal sea surface.

### 2.2. Nonlinear fractal sea surface

Assuming a linear sea surface and based on the basis of long-wave–short-wave interactions, Xie *et al.*[10] presented a model for the nonlinear fractal sea surface as follows:

$$\begin{aligned} &f_{\text{nonlinea}}(x,t) \\ &= \sum_{n=1}^{N}\left(a_n\sin\psi_n - \frac{1}{2}a_n^2 k_n \sin(2\psi_n)\right) - \frac{1}{2(N-N_0)} \\ &\times \sum_{n=N_0+1}^{N}\sum_{m=1}^{N_0} a_n a_m\big[(k_n+k_m)\cos(\psi_n+\psi_m) \\ &+ (k_n-k_m)\cos(\psi_n-\psi_m)\big], \end{aligned} \tag{6}$$

where

$$\begin{aligned} &a_{n,m} = \sigma C b^{(s-2)n,m}, \quad \omega_{n,m} = \sqrt{gk_{n,m}}, \\ &k_{n,m} = k_0 b^{n,m}, \quad \psi_{n,m} = k_{n,m}x - \omega_{n,m}t + \varphi_{n,m}, \end{aligned}$$

$n$ and $m$ refer to the ordinal numbers of $n$-th and the $m$-th waves which correspond to the components of short wave and long wave, respectively, and $N_0$ is the series number of the shortest wavelength in long wave trains. According to the condition of interaction between long wave and short wave,[18] i.e., $k_{N_0+1} \gg k_{N_0}$, where $n$ and $m$ should satisfy the inequalities $n > N_0$ and $m \leq N_0$, where $N_0$ can be determined by the following criterion:

$$b^{(N_0+1)} - b^{(N_0)} \geq 10. \tag{7}$$

### 2.3. One-dimensional nonlinear wave–current coupled fractal sea surface model

Ryu *et al.*[19] developed a numerical wave tank (NWT) with free surface boundary conditions to investigate wave–current interactions and the resulting kinematics. Inspired by their method, we derive a one-dimensional nonlinear wave–current fractal sea surface model in this paper.

A schematic diagram of the numerical wave tank (NWT) and its boundaries are shown in Fig. 1. The left boundary is between the water and the wave generator. The artificial damping zone closes at the right boundary (wall) of the tank. The wave propagates in the $x$ direction on the free surface. The depth of the water is $H$, and $\xi(x,t) = f(x,t)$ is the elevation of the water free surface.

Assuming that the surface current is uniform and $C_0$ is in the $x$ direction, the velocity potential of the sea surface current

is

$$\psi(x,t) = C_0 x + \phi(x,t), \tag{8}$$

where $C_0$ is the velocity of the current. Here, $C_0 > 0$ when the direction of the current is identical to the wave direction, while $C_0 < 0$ means that the current direction is opposite to the wave direction. Here, $\phi(x,t)$ represents the unstable wave potential. Equation (8) satisfies the Laplace equation

$$\nabla^2 \Psi(x,t) = 0. \tag{9}$$

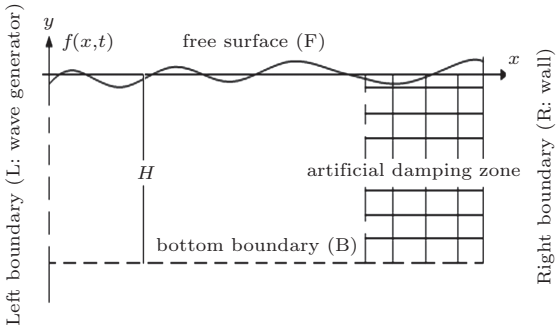



**Fig. 1.** Schematic diagram of the numerical wave tank (NWT) and boundaries.

The wave should be completely dissipated in the artificial damping zone. According to the boundary conditions on the input boundary (L), the wall (R), and the bottom (B), we have

$$\frac{\partial \psi}{\partial n} = C_0 + \frac{\partial \phi}{\partial n} = C_0, \quad \text{on R}, \tag{10}$$

$$\frac{\partial \psi}{\partial n} = -\frac{\partial \phi_{\mathrm{L}}}{\partial n} - C_0, \quad \text{on L}, \tag{11}$$

$$\frac{\partial \psi}{\partial n} = \frac{\partial \phi_{\mathrm{B}}}{\partial n}, \quad \text{on B}. \tag{12}$$

The kinematic free surface boundary conditions are

$$\frac{Dx}{Dt} = \frac{\partial \psi}{\partial x}, \tag{13}$$

$$\frac{Dy}{Dt} = \frac{\partial \psi}{\partial y}, \tag{14}$$

where

$$\frac{D}{Dt} = \frac{\partial}{\partial} + \nabla\psi \cdot \nabla. \tag{15}$$

Sea surface velocity is caused by the motion of free surface water particles; from Eqs. (13)–(15), one can obtain

$$\frac{\partial \xi}{\partial x} = -\frac{\partial \psi_{\mathrm{F}}}{\partial x}\frac{\partial \xi}{\partial x} + \frac{\partial \psi_{\mathrm{F}}}{\partial \xi}. \tag{16}$$

Substituting Eq. (3) into Eq. (16) yields

$$\frac{\partial \xi}{\partial t} = -\frac{\partial \phi_{\mathrm{F}}}{\partial x}\frac{\partial \xi}{\partial x} + \frac{\partial \phi_{\mathrm{F}}}{\partial \xi} - C_0\frac{\partial \xi}{\partial x}. \tag{17}$$

Assuming that the pressure on the free surface is uniform, which is equal to the atmospheric pressure, the Bernoulli equation on the free surface becomes

$$\frac{\partial \psi}{\partial t} + \frac{1}{2}|\nabla\psi|^2 + g\xi + \frac{P_{\mathrm{a}}}{\rho} = 0, \tag{18}$$

where $\rho$ is the water density. Let the atmospheric pressure $P_{\mathrm{a}}$ be zero and substitute Eq. (8) into Eq. (18), then we will have

$$\frac{\partial \phi_{\mathrm{F}}}{\partial t} = -g\xi - \frac{1}{2}\left[\left(\frac{\partial \phi_{\mathrm{F}}}{\partial x}\right)^2 + \left(\frac{\partial \phi_{\mathrm{F}}}{\partial \xi}\right)^2\right] - C_0\frac{\partial \phi_{\mathrm{F}}}{\partial x}. \tag{19}$$

Using initial conditions $\phi = 0$ in the water domain and $\xi = 0$ at $t = 0$, equation (19) can be solved as

$$\psi(x,t) = C_0 x + \frac{ga\cosh\{k(\xi+H)\}}{\omega\cosh(kH)}\sin(kx - \omega t) \tag{20}$$

with $H \gg \xi$ in deep sea. Equation (20) can be simplified into

$$\psi(x,t) = C_0 x + \frac{ga}{\omega}\sin(kx - \omega t), \tag{21}$$

where $a$ is the wave amplitude. Therefore, the dispersion relation for the wave–current coupled dynamics in deep water can be written as

$$(\omega - kC_0)^2 = kg, \tag{22}$$

and the sea surface can be characterized as

$$\xi(x,t) = a\left(1 - \frac{kC_0}{\omega}\right)\cos(kx - \omega t + \varphi). \tag{23}$$

Substituting Eq. (23) into Eq. (2), we can obtain the solution for the linear wave–current model as follows:

$$f_{\mathrm{linear}}(x,t) = \sum_{n=0}^{N-1} \sigma C b^{(s-2)n}\left(1 - \frac{K_0 b^n C_0}{\omega_n}\right) \times \sin K_0 b^n x - \omega_n t + \varphi_n. \tag{24}$$

However, the real sea surface is generally nonlinear. Therefore, it is necessary to investigate the nonlinear wave–current model.

Considering nonlinear wave–wave interaction between the long wave and short wave, the nonlinear fractal sea surface model is derived as given in Eq. (6). Using Eqs. (21)–(23) and Eq. (6), one can establish the nonlinear wave–current model as follows:

$$f_{\mathrm{nonlinear}}(x,t) = f^{+}_{\mathrm{nonlinear}}(x,t) + f^{-}_{\mathrm{nonlinear}}(x,t), \tag{25}$$

where

$$\begin{aligned} & f^{\pm}_{\mathrm{nonlinear}}(x,t) \\ &= \sum_{n=1}^{N}\left(a_n^{\pm}\sin\psi_n^{\pm} - \frac{1}{2}(a_n^{\pm})^2 k_n \sin(2\psi_n^{\pm})\right) - \frac{1}{2(N-N_0)} \\ &\times \sum_{n=N_0+1}^{N}\sum_{m=1}^{N_0} a_n^{\pm}a_m^{\pm}\left[(k_n + k_m)\cos(\psi_n^{\pm} + \psi_m^{\pm})\right. \\ &\left. + (k_n - k_m)\cos(\psi_n^{\pm} - \psi_m^{\pm})\right], \end{aligned} \tag{26}$$

where $\omega^{+}_{n,m} = k_{n,m}C_0 + \sqrt{k_{n,m}g}$, $\omega^{-}_{n,m} = k_{n,m}C_0 - \sqrt{k_{n,m}g}$, $k_{n,m} = K_0 b^{n,m}$, $a^{\pm}_{n,m} = \sigma C b^{(s-2)n,m}(1 - K_0 b^{n,m} C_0/\omega^{\pm}_{n,m})$, $\psi^{\pm}_{n,m} = K_0 b^{n,m} x - \omega^{\pm}_{n,m} t + \varphi_{n,m}$, $1 \le m \le N_0$ and $N_0 + 1 \le n \le N$.

## 3. Relative error analysis

To estimate the accuracy of our wave–current couple model, wave amplitude is selected to numerically calculate relative error.

Longuet-Higgins and Stewart[18] suggested that the variation in energy of the short wave is caused by the work done by the long wave against the radiation stress of the short wave. According to the Longuet-Higgins and Stewart study, orbital velocities near the free surface have the horizontal component

$$U_0 = a\omega \coth(kh)\sin\Psi, \tag{27}$$

where $\Psi = Kx - \omega t + \varphi$, $h$ is the depth of water, and the vertical component is

$$V = a\omega\cos\Psi. \tag{28}$$

When the wave rides on current $C_0$, the horizontal component of orbital relative velocity near the free surface can be expressed as

$$U = U_0 - C_0 = a\omega\coth(kh)\sin\Psi - C_0. \tag{29}$$

From Eq. (5.16) of Ref. [19] by Longuet-Higgins and Stewart and Eqs. (28) and (29), one can obtain the wave amplitude changes as given below

$$\frac{a'}{a} = 1 + \frac{ak(3\coth(kh) + \tanh(kh))\sin\Psi}{4} - \frac{3kC_0}{4\omega}, \tag{30}$$

where $a'$ is the effect of the ocean surface current $C_0$ on the wave amplitude. The above equation becomes

$$\frac{a'}{a} = 1 + ak\sin\Psi - \frac{3kC_0}{4\omega}, \tag{31}$$

when one considers the wave riding on the surface of deep water.

The relative error $e_r$ of the difference between the wave amplitude in deep water from our model and that from the analytic solution by Longuet-Higgins MS and Stewart,[18] is

$$e_r = 1 - \frac{1 - \dfrac{kC_0}{\omega}}{1 + ak\sin\Psi - \dfrac{3kC_0}{4\omega}}. \tag{32}$$

Equation (32) is used to calculate relative error in the wave amplitude in our model. The root-mean-square (RMS) wave amplitude errors can also easily be obtained based on the relative errors. As an example, figure 2 shows the relation between sea surface current speed and the RMS relative wave amplitude errors when wave amplitude is 2 m, wave length is 200 m, and sea surface currents range from $-2\ \mathrm{m\cdot s^{-1}}$ to $2\ \mathrm{m\cdot s^{-1}}$. This range covers most of the ocean surface currents in the world.

Figure 2 shows that the RMS relative wave amplitude error increases with increasing sea surface current magnitude. The maximum RMS of relative error is 5.52% when $C_0 = 2\ \mathrm{m\cdot s^{-1}}$. The minimum RMS of relative error is 445% when $C_0 = -0.10\ \mathrm{m\cdot s^{-1}}$. Being relative to the other uncertainties in simulations of ocean waves and wave–current interactions, such as errors in wind fields, unknown physics for wave dissipation, it is acceptable for the model simulation to have a relative error that is less than 10%. Thus, our model presents the results in good agreement with the theoretical results.

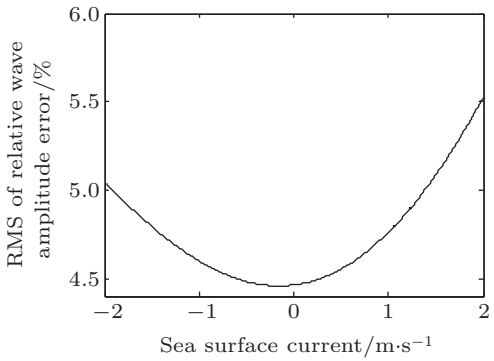



**Fig. 2.** Relation between RMS relative wave amplitude error and sea surface current velocity.

Moreover, the limit of the possible numerical application of our model is studied here. According to Stokes wave theory, the maximum steepness of ocean wave is 0.142. Therefore we let wave steepness increase from 0 to 0.142, and let the velocities of sea surface currents range from $-2\ \mathrm{m\cdot s^{-1}}$ to $2\ \mathrm{m\cdot s^{-1}}$. Therefore, the RMS relative wave amplitude error varies with wave steepness and velocity of sea surface current as shown in Fig. 3. The white color in Fig. 3 indicates the case where the RMS relative wave amplitude error is larger than 10%.

Numerical results show that our model can simulate 92% of the case shown in Fig. 3. In other words, the relative error of our model is less than 10% for sea surface current velocity varying over the range from $-2\ \mathrm{m\cdot s^{-1}}$ to $2\ \mathrm{m\cdot s^{-1}}$ and for ocean wave steepness less than 0.142.

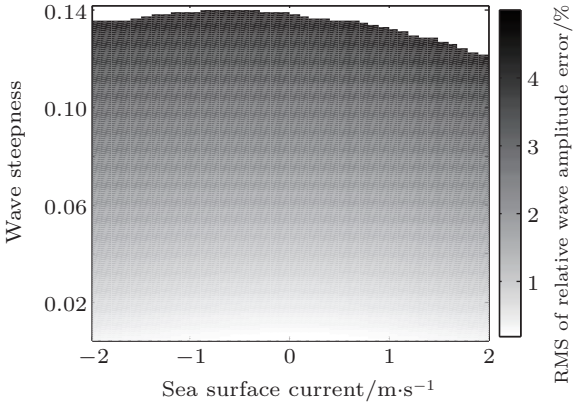



**Fig. 3.** Variation of RMS relative wave amplitude error with wave steepness and sea surface current velocity.

## 4. Numerical results and discussion

To find the differences between the current effect on the nonlinear sea surface model and that on its wave–current cou-

pled model, the initial conditions are set to be the same as previous ones, i.e., $x = 1$ m, $\lambda_0 = 200$ m, $b = 2e/3$, $\sigma = 075$, $s = 13$, and $N = 25$. According to Eq. (7), one can obtain $N_0 = 6$. Therefore, all wave components are long waves when $N \leq 6$ and the wave components are short waves when $N > 6$.

### 4.1. Effect of current on the wave

#### 4.1.1. The effects of currents on wave amplitude and wavelength

The effect of ocean surface current on wave amplitude is investigated here. Suppose that the velocity of the ocean surface current is positive when the current direction is the same as the wave propagation direction, and negative when the current direction is opposite to the wave propagation direction. Let $C_0 = \pm 0.5$ m·s$^{-1}$ and $C_0 = 0$ m·s$^{-1}$; the effects of current on the wave amplitude for different cases are shown in Fig. 4.

The effects of current on wave amplitude are shown in Fig. 4. Figure 4(a) shows that the wave amplitude increases with increasing wavelength when $C_0 = 0$ m·s$^{-1}$. Compared with the case where there is no current nor drifting sea surface, wave amplitude decreases when the wave propagates in the same direction as the current direction (for example, $C_0 = 0.5$ m·s$^{-1}$) whereas wave amplitude increases when the wave propagates in the opposite direction to the current direction (for example, $C_0 = -0.5$ m·s$^{-1}$). The relative variations of wave amplitude with wavelength corresponding to Fig. 4(a) are shown in Fig. 4(b). From Fig. 4(b), one can find that the effects of current on wave amplitude decrease with increasing wavelength. The effects of current on wave amplitude when wavelengths are less than 50 m are much greater than those when wavelengths are more than 50 m. The maximum relative changes in wave amplitude are 15% ($C_0 = -0.5$ m·s$^{-1}$) and $-21.5\%$ ($C_0 = 0.5$ m·s$^{-1}$), respectively. Wave amplitudes decrease to 4.3% and $-2.9\%$ when wavelength increases to 50 m, respectively. Figure 4(c) shows the variations of wave amplitude with ocean current velocity for different wavelengths. The variations of relative wave amplitudes with ocean current velocity for different wavelengths corresponding to those in Fig. 4(c) are shown in Fig. 4(d). Results show that wave amplitude increases when $C_0 < 0$ m·s$^{-1}$ while wave amplitude decreases when $C_0 > 0$ m·s$^{-1}$ at different wavelengths. In comparison to short waves, the effects of current on long wave amplitude are less than those of short wave.

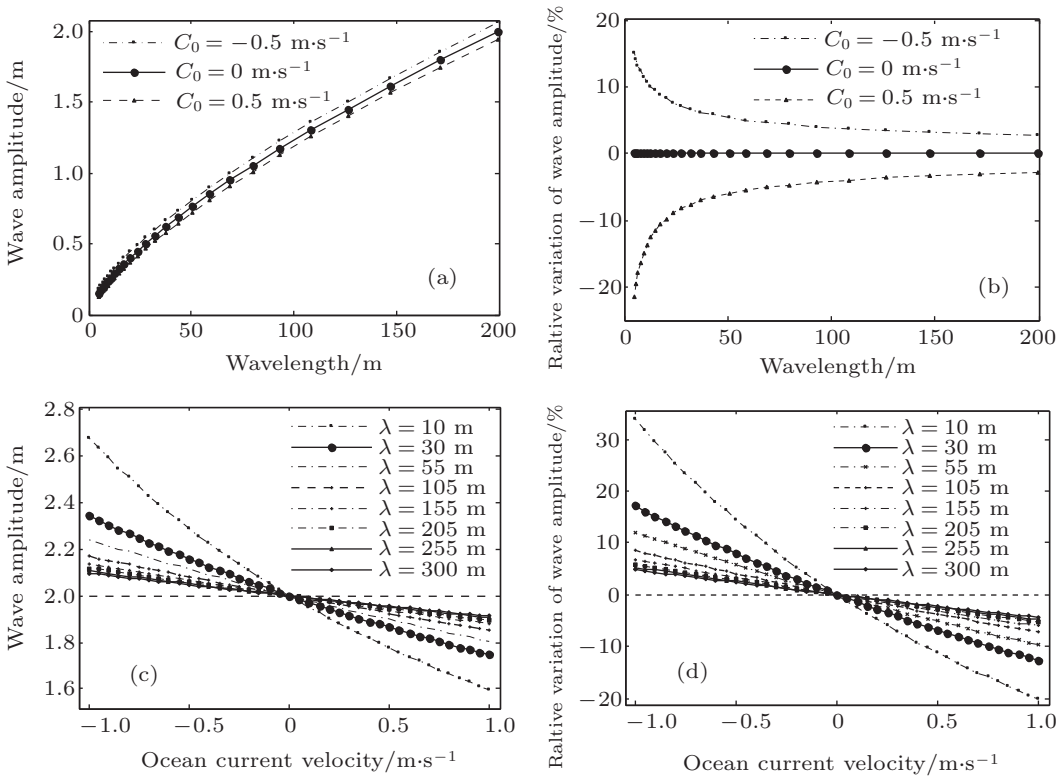



**Fig. 4.** Effects of current on wave amplitude, showing (a) variations of wave amplitude with wavelength for different directions of current velocity; (b) variations of percentage of relative wave amplitude with wavelength for different directions of current velocity corresponding to those in panel (a); (c) variations of wave amplitude with current velocity for different wavelengths; (d) variations of percentage of relative wave amplitude with current velocity for different wavelengths corresponding to those in panel (c).

The effects of current on wave wavelength are shown in Fig. 5. Figure 5(a) shows that the wavelength increases when wave propagates in the same direction as the current direction (for example, $C_0 = 0.5$ m·s$^{-1}$), whereas wavelength decreases when the wave propagates in the opposite direction to the current direction (for example, $C_0 = -0.5$ m·s$^{-1}$). The relative variations of the wavelength affected by current with wavelength for different current velocities corresponding to those in

Fig. 5(a) are shown in Fig. 5(b). From Fig. 5(b), one can find that the effect of current on wavelength decreases with increasing wavelength. The effects of current on wavelength when wavelengths are less than 50 m are much greater than when wavelengths are more than 50 m. The maximum changes of wave amplitude are 27.8% for current $C_0 = 0.5$ m·s$^{-1}$, and $-47.6\%$ for the opposite current $C_0 = -0.5$ m·s$^{-1}$ respectively. Wavelengths decrease to 10.4% and $-12.3\%$ when wavelength increases to 50 m for the parallel and opposite currents, respectively, compared with 5.4% and $-5.9\%$ when wavelength increases to 200 m. The changes of wavelength and their relative variation affected by ocean current are shown in Figs. 5(c) and 5(d), respectively. Results show that wavelength is shortened in opposing current and lengthened in collinear current. The overall effect of current on long waves is less than the effect on short waves.

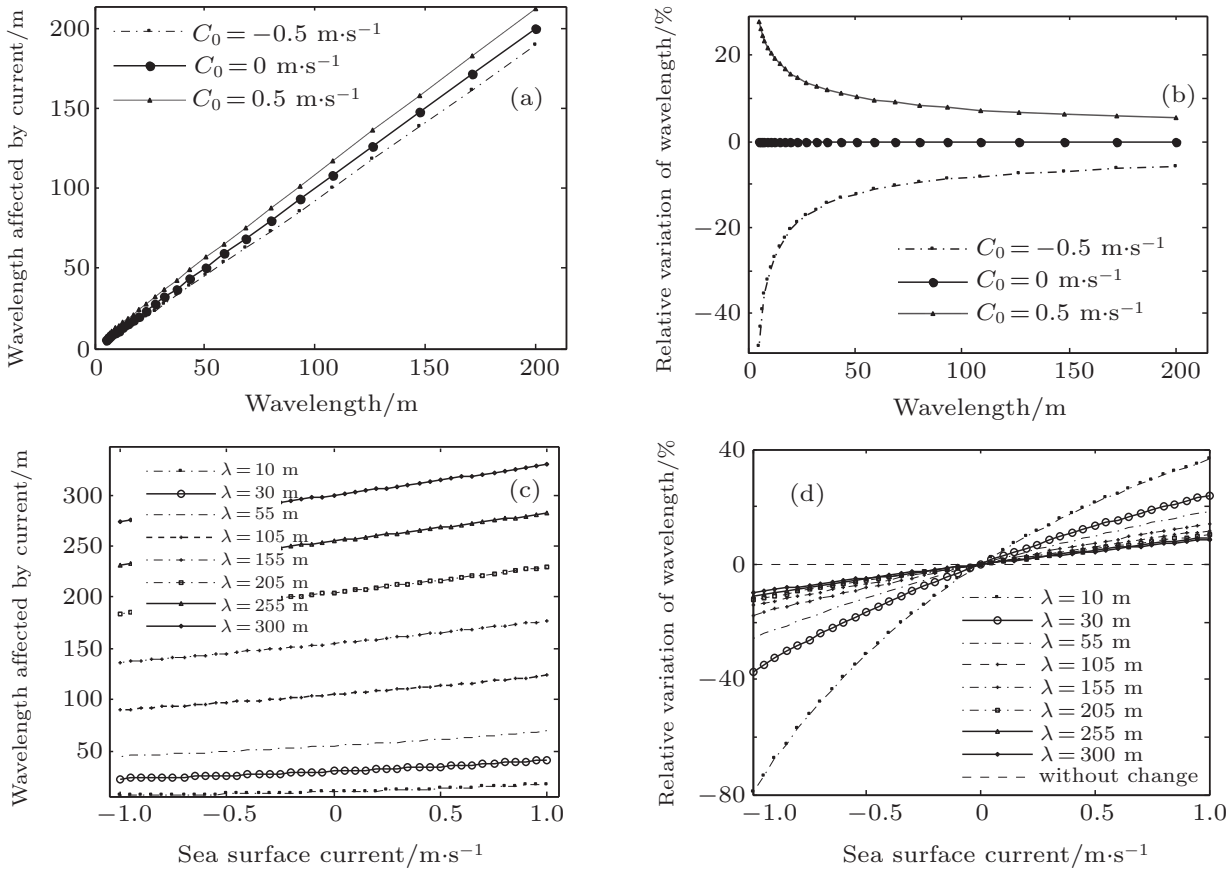



**Fig. 5.** Effects of current on wave wavelength, showing (a) variations of wavelength affected by current with wavelength for different directions of current velocity; (b) variations of relative variation of wavelength with wavelength for different directions of current velocity corresponding to those in panel (a); (c) variations of wavelength affected by current with sea surface current velocity for different wavelengths; (d) variations of the relative variation of wavelength with sea surface current velocity corresponding to those in panel (c).

### 4.1.2. Effects of currents on wave heights

We now choose the following parameters:

$$C_0 = \pm 0.2 \text{ m·s}^{-1},\ b = 2e/3,\ \sigma = 0.75,\ s = 1.3,\ N = 25.$$

To ensure enough samples, the simulation time interval is set to be $t = [001 \text{ s}, 3363 \text{ s}]$, which is 300 times the dominant period. The simulation time step is 0.01 s in this work. Thus, 336300 samples are obtained.

As an example, consider currents of $C_0 = \pm 0.6$ m·s$^{-1}$ and $C_0 = 0$ m·s$^{-1}$ on linear and nonlinear fractal sea surfaces respectively. The wave height evolutions with time are shown in Fig. 6, where figures 6(a)–6(c) show the results of the linear fractal sea surfaces and figures 6(d)–6(f) display the results for the nonlinear fractal sea surface. Different current velocities are included.

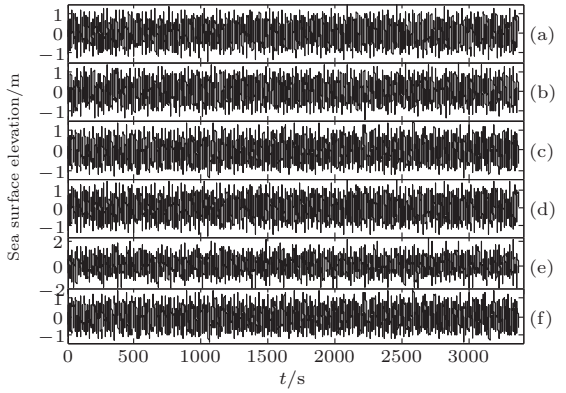



**Fig. 6.** Wave height evolutions with time, showing (a) linear fractal sea surface without current; (b) linear fractal sea surface with current $C_0 = 0.6$ m·s$^{-1}$; (c) linear fractal sea surface with current $C_0 = -0.6$ m·s$^{-1}$; (d) nonlinear fractal sea surface without current; (e) nonlinear fractal sea surface with current $C_0 = 0.6$ m·s$^{-1}$; (f) nonlinear fractal sea surface with current $C_0 = -0.6$ m·s$^{-1}$.

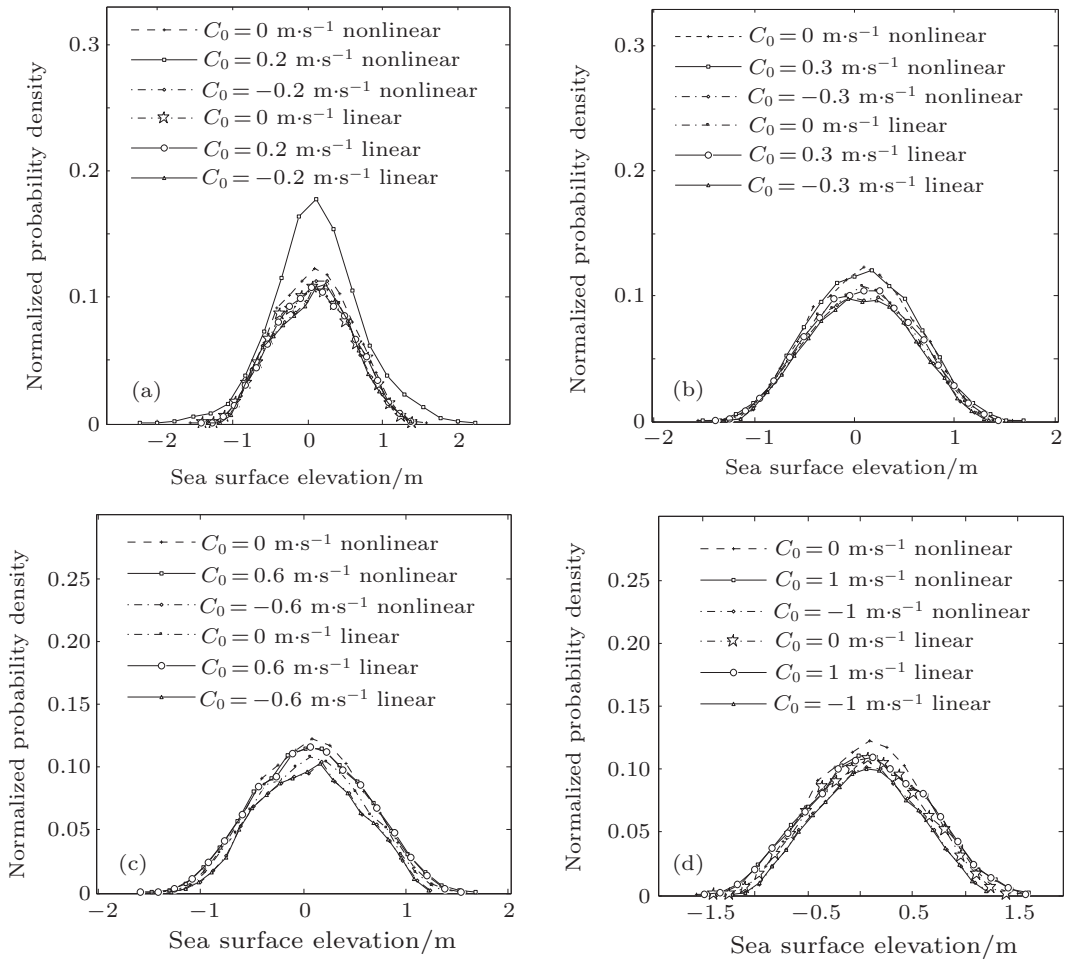



**Fig. 7.** Normalized probability density distributions for wave heights of a fractal sea surface for different current velocities: (a) $C_0 = \pm 0.2$ m·s$^{-1}$; (b) $C_0 = \pm 0.3$ m·s$^{-1}$; (c) $C_0 = \pm 0.6$ m·s$^{-1}$; (d) $C_0 = \pm 1$ m·s$^{-1}$.

Results in Fig.6 are used to generate statistics and analyze the normalized probability density function (PDF) for wave heights which are shown in Fig. 7, where figures 7(a)–7(d) show the normalized wave height PDFs for the linear and nonlinear fractal sea surface with current velocities of $C_0 = \pm 0.2$ m·s$^{-1}$, $C_0 = \pm 0.3$ m·s$^{-1}$, $C_0 = \pm 0.6$ m·s$^{-1}$, and $C_0 = \pm 1$ m·s$^{-1}$, correspondingly. Each of the PDF curves in Fig. 7 has characteristics of a Gaussian curve.

**Table 1.** Values of kurtosis and skewness of PDF of the fractal sea surface wave height affected by different current velocities.

| Current velocity $C_0$/m·s$^{-1}$ | Linear fractal sea surface | | Nonlinear fractal sea surface | |
|---|---|---|---|---|
| | $\beta$ | $\alpha$ | $\beta$ | $\alpha$ |
| –1.0 | 2.379 | –0.008 | 2.379 | 0.001 |
| –0.6 | 2.356 | –0.004 | 2.357 | –0.002 |
| –0.3 | 2.362 | –0.001 | 2.363 | 0.002 |
| –0.2 | 2.400 | –0.001 | 2.402 | 0.002 |
| 0 | 2.411 | 0.001 | 2.467 | 0.005 |
| 0.2 | 2.424 | –0.004 | 3.459 | 0.097 |
| 0.3 | 2.432 | –0.009 | 2.509 | 0.014 |
| 0.6 | 2.449 | 0.003 | 2.479 | 0.031 |
| 1.0 | 2.473 | –0.007 | 2.492 | 0.033 |

The values of kurtosis ($\beta$) and skewness ($\alpha$) of the wave height PDF of the fractal sea affected by different current velocities in Fig. 7 are listed in Table 1. From Table 1, one can find that PDF distributions of both nonlinear and linear fractal sea surface wave height have positive skewness distributions ($\alpha > 0$) when $C_0 = 0$ m·s$^{-1}$, where values of $\alpha$ are changed by current velocity. Here, $\beta$ is defined as the discrepancy between the fourth order central moment and the kurtosis of the Gaussian distribution (which is 3), i.e., $\beta = \text{Kurtosis} - 3$. Therefore, $\beta$ is also affected by currents which can also be seen in Table 1.

The effective trends of current on kurtosis and skewness of wave height distributions on the linear and nonlinear fractal sea surface are shown in Fig. 8. Ocean current velocity increases from $-2$ m·s$^{-1}$ to 2 m·s$^{-1}$ here. The original $\beta$ and $\alpha$data are shown in Figs. 8(a) and 8(c), respectively. Fitted curves corresponding to Fig. 8(a) and Fig. 8(c) are shown in Figs. 8(b) and 8(d), respectively.

The results in Fig. 8(b) show that for the nonlinear fractal sea surface, the kurtosis of wave height PDF is larger than that of the linear fractal sea surface, under the same currents. Moreover, the kurtosis increases with increasing current velocity. While the skewness interval of the wave height PDF shown in Fig. 8(d) is small, ranging from $-0.2$ to 0.25, which is much smaller than that of the general PDF, ranging from -3 to 3, the effect of current on the skewness of the wave height PDF is relatively small.

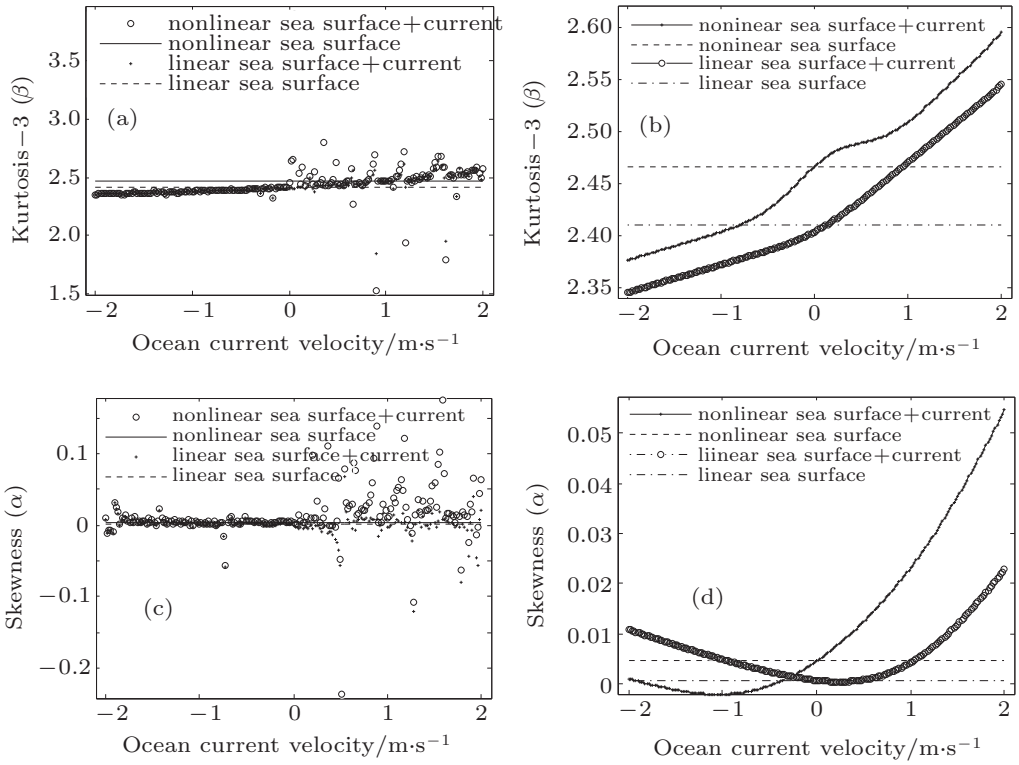



**Fig. 8.** Variations of kurtosis and skewness of wave height PDF with ocean current velocity, showing (a) variations of original $\beta$ with current; (b) fitted $\beta$ curves corresponding to the cases in panel (a); (c) variations of original $\alpha$ with current; (d) fitted $\alpha$ curves corresponding to the cases in panel (c).

### 4.2. Effect of current on wave spectrum

Results in Fig. 9 show that currents can affect wave spectra of both the linear (Fig. 9(a)) and nonlinear (Fig. 9(b)) fractal sea surface. Differences in wave spectrum between the nonlinear and linear sea surface are shown in Fig. 9(c).

It is shown in both Figs. 9(a) and 9(b) that wave spectrum intensities are strengthened when waves propagate in opposing currents ($C_0 = -1$ m·s$^{-1}$ in Fig. 9). However, the spectrum peaks shift towards higher frequencies. Therefore, the peak wave lengths must be shortened. Moreover, the wave spectra are weakened in collinear current ($C_0 = 1$ m·s$^{-1}$ in Fig. 9). In other words, the peak wave lengths are lengthened.

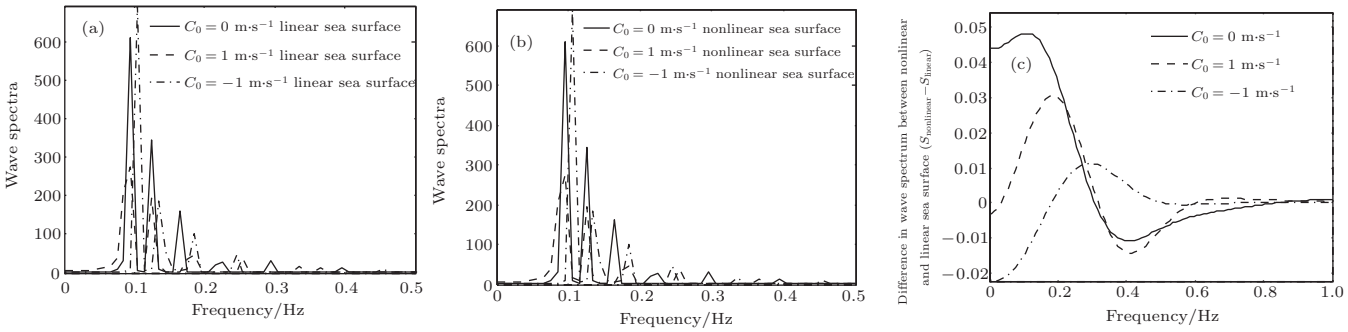



**Fig. 9.** Wave spectra for current velocities of $-1$ m·s$^{-1}$, 0 m·s$^{-1}$, and 1 m·s$^{-1}$ on (a) linear sea surface and (b) nonlinear sea surface; (c) Difference in wave spectrum between the nonlinear and the linear sea surface $S_{\text{nonlinear}}$–$S_{\text{linear}}$.

The differences in spectrum between linear and nonlinear fractal sea surfaces, for different current velocities, are shown in Fig. 9(c). The peak spectra for the linear sea surface case, at currents $-1$ m·s$^{-1}$ and 1 m·s$^{-1}$, are 692.6 and 273.7, respectively. The difference is 418.9. The corresponding difference is 418.6 for the nonlinear fractal sea surface. Comparing the effects of current on wave spectrum for linear and nonlinear sea surfaces, the effect of the nonlinearity on the wave spectrum can be ignored.

## 5. Conclusions

A wave–current coupled model is established in this paper. The model is used to numerically study the effect of the current on the wave.

Numerical simulation results show that the wave amplitude decreases (increases) when the wave propagates in the direction the same as (opposite to) the current direction. Wavelength and wave height kurtosis increase, whereas wave spectrum intensity decreases and shifts towards lower frequencies

when current direction is parallel to the ocean wave direction. By comparison, if current direction is opposite to the the wave direction, then wave amplitude increases, wavelength and wave height kurtosis decrease, and spectrum intensity increases and shifts towards higher frequencies. The effect of ocean current is much stronger than that of a nonlinear wave. The kurtosis of the nonlinear fractal ocean surface is larger than that of the linear fractal ocean surface. The effect of current on the skewness of the probability distribution function is negligible.

Our results imply that the ocean wave spectrum distribution is changed by ocean surface currents, which must be reflected in electromagnetic backscattering observations. An electromagnetic backscatter model of the effect of current on fractal sea surface is established in Part 2 of this study, based on the wave–current coupled model presented in this paper (Part 1).

## References


[1] Yoder J A, Doney S C, Siegel D A and Wilson C 2010 *Oceanography* **23** 104

[2] Chapron B, Collard F and Ardhuin F 2005 *J. Geophys. Res.* **110** C07008

[3] Johannessen J A, Chapron B, Collard F, Kudryavtsev V, Mouche A, Akimov D and Dagestad K F 2008 *Geophys. Res. Lett.* **35** L22608

[4] Marghany M 2011 *J. Phys. Sci.* **6** 6630

[5] Hansen M W, Collard F, Dagestad K, Johannessen J A, Fabry P and Chapron B 2011 *IEEE Trans. Geosci. Remote Sens.* **49** 103582

[6] Rossi C, Runge H, Breit H and Fritz T 2010 IGARSS'10, July 25–30, Hawaii, USA, p. 3055

[7] Zhang F W, Drennan W M, Haus B K and Graber H C 2009 *J. Geophys. Res.* **114** C01018

[8] Smith J A 2006 *J. Phys. Oceano.* **36** 1403

[9] Yu J and Slinn D N 2003 *J. Geophys. Res.* **108** C3 3088

[10] Xie T, Zou G, Perrie W, Kuang H and Chen W 2010 *Chin. Phys. B* **19** 059201

[11] Guo L, Wang Y and Wu Z 2005 *Acta Phys. Sin.* **54** 96 (in Chinese)

[12] Yang J, Guo L and Wan J 2007 *Acta Phys. Sin.* **56** 2106 (in Chinese)

[13] Tian W, Ren X and Guo L 2012 *Systems Engineering and Electronics* **34** 1775 (in Chinese)

[14] Tao R, Li Y, Bai X and Waheed A 2012 *IEEE Trans. Geosci. Remote Sens.* **50** 3627

[15] Wang C, Feng W and Li C 2013 *J. B. Univ. Aeronaut. Astronaut.* **39** 1212 (in Chinese)

[16] Luo F, Zhang D and Zhang B 2013 *IEEE Geosci. Remote Sens. Lett.* **10** 1295

[17] Chen Y, Hu Y, Lin T and Wang H 2014 *J. N. Univ. Sci. Tech.* **38** 140 (in Chinese)

[18] Longuet-Higgins M S and Stewart R W 1960 *J. Fluid Mech.* **8** 565

[19] Ryu S, Kim M H and Lynett P J 2003 *Comput. Mech.* **32** 336